Journal of Sound and Vibration 329 (2010) 4643–4655

Contents lists available at ScienceDirect

Journal of Sound and Vibration

journal homepage: www.elsevier.com/locate/jsvi

A finite element study on rail corrugation based on saturated creep force-induced self-excited vibration of a wheelset–track system

G.X. Chen [a], Z.R. Zhou [a,*], H. Ouyang [b], X.S. Jin [a], M.H. Zhu [a], Q.Y. Liu [a]

[a] Tribology Research Institute, State Key Laboratory of Traction Power, Southwest Jiaotong University, Chengdu 610031, China
[b] Department of Engineering, University of Liverpool, Brownlow Street, Liverpool L69 3GH, UK

ARTICLE INFO

Article history:
Received 25 April 2009
Received in revised form
11 May 2010
Accepted 14 May 2010
Handling Editor: M.P. Cartmell
Available online 9 June 2010

ABSTRACT

The present work proposes friction coupling at the wheel–rail interface as the mechanism for formation of rail corrugation. Stability of a wheelset–track system is studied using the finite element complex eigenvalue method. Two models for a wheelset–track system on a tight curved track and on a straight track are established. In these two models, motion of the wheelset is coupled with that of the rail by friction. Creep force at the interface is assumed to become saturated and approximately equal to friction force, which is equal to the normal contact force multiplied by dynamic coefficient of friction. The rail is supported by vertical and lateral springs and dampers at the positions of sleepers. Numerical results show that there is a strong propensity of self-excited vibration of the wheelset–track system when the friction coefficient is larger than 0.21. Some unstable frequencies fall in the range 60–1200 Hz, which correspond to frequencies of rail corrugation. Parameter sensitivity analysis shows that the dynamic coefficient of friction, spring stiffness and damping of the sleeper supports all have important influences on the rail corrugation formation. Bringing the friction coefficient below a certain level can suppress or eliminate rail corrugation.

1. Introduction

Nowadays, the impact of rail corrugation is not as strong as before since grinding is generally used to remove rail corrugation of all types of rails all over the world. However, rail corrugation is still an elusive problem in the railway industry. Grinding is a passive and expensive method. Eliminating or suppressing corrugation is still the best solution. Over the years, many efforts have been made to understand the formation mechanisms of various types of corrugation. Grassie and Kalousek [1] appear to be two of the first researchers to propose the classification of rail corrugation in terms of wavelength-fixing and damage mechanisms, which is helpful to the understanding of rail corrugation mechanisms. Grassie and Kalousek [1], Grassie [2], Sato et al. [3], Ahlbeck and Daniels [4], Knothe [5] and Oostermeijer [6] published several comprehensive reviews. In these reviews, several mechanisms of corrugation formation were summarized, including the self-excited rutting-type corrugation due to negative damping of friction, torsional vibration of wheelset, instability similar to hunting motion and P2 resonance of the unsprung mass on track stiffness. These proposed generation mechanisms of rail corrugation can be roughly grouped into two major schools of thought. First, it is commonly believed that rail corrugation is caused by a combination of transient dynamic interaction between the wheel and rail and long term wear. A basic assumption in this school of thought is that the original rail head has discontinuities as a result of production and construction. This unevenness causes excitations to result in fluctuations of contact forces when a wheel rolls over a rail.

* Corresponding author. Fax: +86 028 87600971.
E-mail address: zrzhou@swjtu.edu.cn (Z.R. Zhou).

0022-460X/$ - see front matter © 2010 Elsevier Ltd. All rights reserved.
doi:10.1016/j.jsv.2010.05.011

Under conditions of large creepages, fluctuating contact forces cause different wear rates of rail running surfaces to generate corrugation. Hempelmann and Knothe [7], Igeland and Ilias [8] and Matsumoto and Sato [9] were the early advocates of this school of thought. Their work has led to the development of integrated simulation programs incorporating dynamics of the track and discrete element models for rolling contact mechanics. Vadillo et al. [10] found that corrugation would cease when an intermediate sleeper was installed between each two sleepers. Hempelmann and Knothe [7] considered vertical 'pinned–pinned resonance' to be the most likely source for corrugation. Ilias [11] found that stiffer pads led to higher differential wear rates and therefore faster corrugation growth. Muller [12] and Nielsen [13] investigated a nonlinear contact mechanics filter and used it to explain the independence of wavelength with respect to speed for short pitch corrugation. Andersson and Johansson [14] developed a three-dimensional model to enable corrugation studies on both tangent and curved tracks. Wu and Thompson [15] numerically investigated the effect of multiple wheel–track passes using a frequency domain model. Jin et al. [16,17] and Jin and Wen [18] developed a more complicated rail corrugation model that combined Kalker's rolling contact mechanics with non-Hertzian form, a linear frictional work and dynamics of half a railway vehicle coupled with curved tracks. Using the model, Jin and Wen [18] found that discrete sleeper supports were a main cause of rail corrugation on curved tracks.

Secondly, rail corrugation is believed to be due to instability of wheel–rail systems. Although the investigators who accept this point of view are fewer than those who accept the first point of view, the impact of this school of thought continues to date. Clark [19] and Clark et al. [20]earlier investigated rail corrugation from the view point of stick–slip. Brockley [21] studied the influence of friction-induced vibration on rail corrugation and derived a formula expressing the relation between corrugation wear and friction-induced vibration. Muller [12] investigated stability of the feedback loop of transient wheel–track dynamics. Ishida et al. [22] considered that fluctuation of Q/P (lateral/vertical forces) might lead to stick–slip between rail and wheel and wear took place to form corrugation. Yoshihiro Suda et al. [23] and Matsumoto et al. [24] also attributed rail corrugation to stick–slip. Wu and Thompson [25] investigated rail corrugation due to micro-slip. Most recently, Sun and Simson [26] studied wagon–track modeling and parametric sensitivity on rail corrugation initiation due to wheel stick–slip. They found that low static friction made the creepage easily overcome the wheel–rail interface's ability to accommodate it, thus leading to the wheel stick–slip process. Further, low kinetic friction coefficient intensified the wheel stick–slip process.

Nevertheless, the generation mechanism of rail corrugation does not appear to be fully known. For example, the existing rail corrugation theories cannot be used to satisfactorily explain the mechanism of friction modifiers (FMs), which suppress rail corrugation as Grassie [2] suggested. Several investigators reported that bringing the coefficient of friction below a level of about 0.35 might effectively suppress wear-type corrugation using friction modifiers [27–29]. Most recently, Eadie et al. [27] reported that in most cases there was little or no new corrugation when FM was applied on sites where corrugation formed rapidly under baseline conditions. He commented that in such a condition wear as a damage mechanism alone was not sufficient to explain the cause. Daniel et al. [30] applied two rail corrugation models to analyze the effect of FM on rail corrugation and concluded that FM did reduce rail corrugation. However, it appears that Daniel's work cannot predict elimination of rail corrugation. All these problems on rail corrugation suggest that there is still much work to be done for obtaining a complete understanding of rail corrugation.

In this paper, a self-excited vibration model of a wheelset–track system is established and stability analysis of the model is performed. The authors find that saturated creep force can induce self-excited vibration of a wheelset–track system. The results can be used to explain some phenomena of rail corrugation which the existing theories cannot. Especially, the results may be used to satisfactorily explain why short pitch corrugation generally occurs on low rail of a tight curved track and why a low friction coefficient can eliminate rail corrugation. The object of the present work is to extend understanding of the generation mechanism of rail corrugation and to explore solutions to rail corrugation. The contents of this paper are as follows. First, a brief review of the progress in rail corrugation research and the existing theories is presented. Next, finite element modeling of a wheelset–track system and nominal parameters are presented. In Section 3, numerical results are given. Finally, conclusions close the paper.

2. Finite element modeling of a wheelset–track system

2.1. Interaction between wheel and rail

Generally speaking, wheels are always kept in contact with rails when a train travels on a track. Dynamic simulations of vehicle curve negotiation and field measurements all demonstrate that on curved tracks the leading wheelsets of both the front and rear trucks have positive angles of attack and the trailing wheelsets have positive or negative angles of attack mainly depending on running speed, as shown in Fig. 1a [31]. For a wheelset with a positive angle of attack, lateral creep forces have fixed directions as shown in Fig. 2a. Dynamic simulations also show that when a vehicle negotiates a tight curved track, lateral creep forces of the leading wheelset become generally saturated, that is, equal to normal forces multiplied by the dynamic friction coefficient. In the case of an unpowered wheelset, longitudinal creep force is low. In tight curved tracks, the contact point between the outer wheel of the wheelset and high rail will shift to the flange root for wheel and to the gauge corner for rail, whilst the contact point between the inner wheel and low rail is roughly kept in the vicinity of the center of rail top for rail and of the tread for wheel, as shown in Fig. 2a. In straight tracks, it is assumed

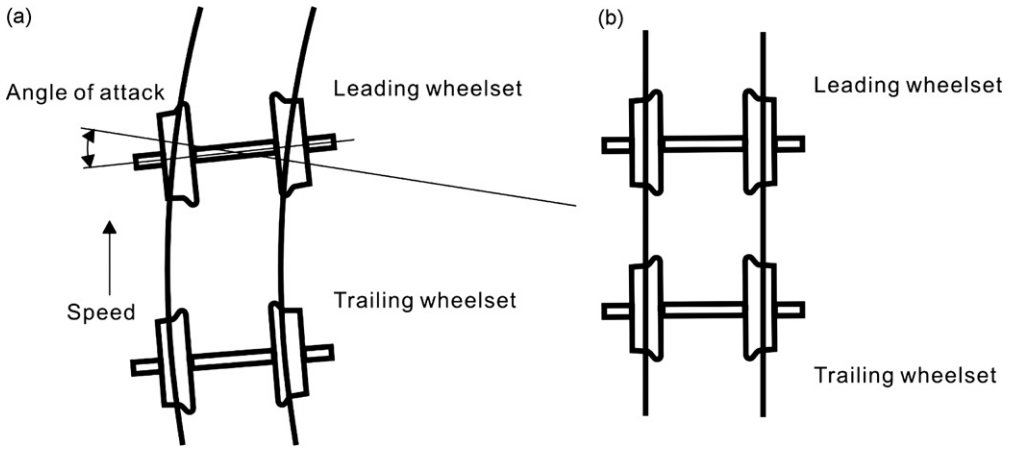

Fig. 1. Wheelset positions: (a) on a tight curved track and (b) on a straight track.

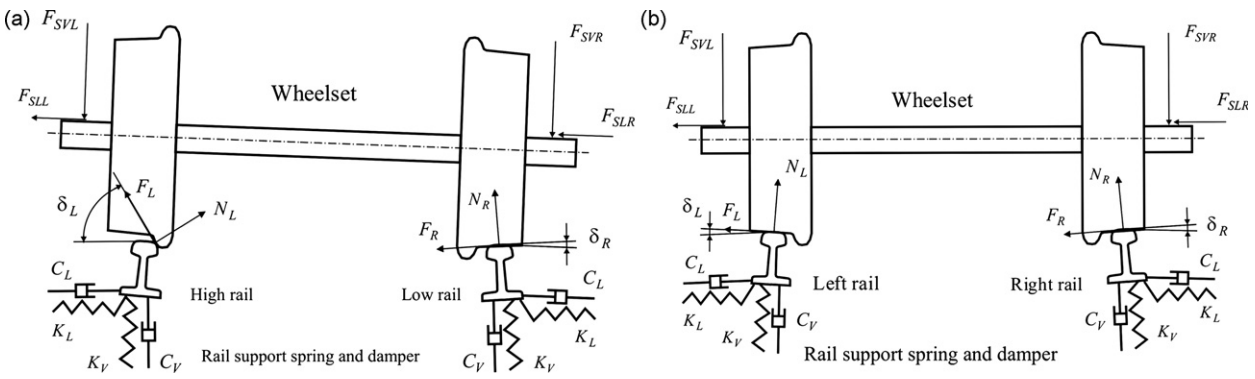

Fig. 2. Positions of contact points and directions of lateral creep forces. In the figures, δ_L and δ_R are the left and the right contact angles, respectively. N_L and N_R are the normal forces at the left and the right contact points, respectively, F_L and F_R the lateral creep forces at the high (left) and the low (right) contact points, respectively, K_V and K_L the vertical stiffness and lateral stiffness of each sleeper support spring, respectively, and C_V and C_L the vertical and lateral damping coefficients of each sleeper support damper, respectively: (a) on a tight curved track and (b) on a straight track.

that there is low lateral displacement of wheelset with respect to the center line of tracks as shown in Fig. 1b. In this case, contact points between the left wheel and rail and between the right wheel and rail are easily determined by contact geometry calculation as shown in Fig. 2b. In the present paper, contact geometry parameters of the wheelset on a curved track are determined by curve negotiation calculation using the NUCARS package [32]. Vehicle and track parameters will be presented in Section 2.5.

2.2. Finite element equations of motion of a wheelset–track system

When a vehicle negotiates a tight curved track or a wheelset undergoes large traction force or brake force on a straight track, creep force between the wheel and rail probably becomes saturated [31]. In the present work, creep forces between the wheels and rails are always assumed to be saturated. In this case, creep forces are similar to friction forces and approximately equal to normal forces multiplied by the dynamic coefficient of friction. In the presence of friction, modeling of the wheelset–track system is very complicated. The complexity is centred in the friction coupling between two elastic bodies. In the literature, there are two approaches available to model friction contact coupling between two elastic bodies [33]. One is based on the massless contact spring assumption at the interface [34,35]. Another is based on Yuan's method, in which there is a constraint on displacements between nodes in contact but no contact spring at the interface [36]. Yuan [36] revealed that massless springs might not be suitable for representing rotor/pads contact at high frequencies. In Yuan's method, contact constraints in the normal direction are mathematically imposed. It may model friction coupling between two elastic bodies more effectively. Yuan's method is introduced briefly as follows [36].

For a friction system shown in Fig. 3, it is assumed that master and slave components are meshed separately with coincident nodes on the interface. The nodes on the sliding surface of the master component are called master nodes, and the ones on the slave component are called slave nodes. Furthermore, the coordinate system for displacement output at

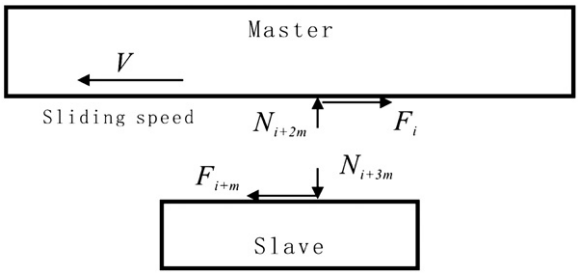

Fig. 3. Schematic of a friction system.

each pair of coincident nodes must be such that one axis points to the positive direction of friction forces on the master node, and another axis is perpendicular to the sliding interface. The axis along the direction of the friction force will be called the tangential axis and the axis normal to the sliding interface will be called the normal axis. It is assumed that there are a total of n degrees of freedom (DOFs) in the system, including $2m$ master and slave nodes on the sliding surfaces. For the convenience of notation, the DOFs are sequenced such that the first m DOFs belong to the master nodes and are along the sliding direction; the second m DOFs belong to the slave nodes and are along the sliding direction too; the third and fourth m DOFs belong to the master and slave nodes, respectively, and are normal to the sliding interface. At the equilibrium position during steady sliding, the following equations must be satisfied:

$$\sum_{j=1}^{n} K_{ij}X_j = F_i, \quad i = 1,2,\ldots,2m \tag{1}$$

$$\sum_{j=1}^{n} K_{ij}X_j = N_i, \quad i = 2m+1,2m+2,\ldots,4m \tag{2}$$

$$\sum_{j=1}^{n} K_{ij}X_j = P_i, \quad i = 4m+1,4m+2,\ldots,n \tag{3}$$

$$F_i + F_{i+m} = 0, \quad i = 1,2,\ldots,m \tag{4}$$

where **K** is the global stiffness matrix, **X** the vector of nodal displacements, **F** and **N** are the vectors of friction and normal contact forces at the master and slave nodes, respectively, and **P** is the vector of external nodal forces. It is assumed that the sliding surfaces do not separate. This contact condition is imposed by the following constraint equations:

$$N_i + N_{i+m} = 0, \quad i = 2m+1,2m+2,\ldots,3m \tag{5}$$

$$X_i - X_{i+m} = 0, \quad i = 2m+1,2m+2,\ldots,3m \tag{6}$$

Note that **P** vanishes in the first $4m$ equations because there are no external loads at the sliding interface. **K** and **P** can be calculated using the finite element method. Friction force on a master node always assumes a positive value because it points to the positive direction of the tangential axis of the output coordinate system. The associated normal contact force also assumes a positive value if the normal axis points to the inside of the master component. Therefore

$$F_i = \mu_i N_{i+2m}, \quad i = 1,2,\ldots,m \tag{7}$$

$$\mu_i = \mu_s + \alpha V_i, \quad i = 1,2,\ldots,m \tag{8}$$

where μ_i is the dynamic coefficient of friction, μ_s the static coefficient of friction, α the slope of friction–velocity curve and V_i the relative sliding speed. Inserting Eq. (2) in Eq. (7) leads to

$$F_i = \mu_i \sum_{j=1}^{n} K_{i+2m,j}X_j, \quad i = 1,2,\ldots,m \tag{9}$$

Finally the equations below are obtained by substituting Eq. (9) for F_i in Eq. (1):

$$\sum_{j=1}^{n} (K_{ij} - \mu_i K_{i+2m,j})X_j = 0, \quad i = 1,2,\ldots,m \tag{10}$$

Similarly, the equations for slave nodes are obtained as follows:

$$\sum_{j=1}^{n} (K_{ij} - \mu_i K_{i+2m,j})X_j = 0, \quad i = m+1,m+2,\ldots,2m \tag{11}$$

Re-writing Eqs. (2) and (3), Eqs. (10) and (11) in matrix form yield

$$(\mathbf{K}+\mathbf{K}_f)\mathbf{X}=\mathbf{P}+\mathbf{N} \tag{12}$$

where $\mathbf{N}$ is a vector of normal contact forces at the interfacial nodes. Matrix $\mathbf{K}_f$, which represents effects of friction, is determined by the friction coefficient. $\mathbf{K}$ is determined according to Eqs. (10) and (11). Normal contact force vector $\mathbf{N}$ and the first m DOFs can be systematically eliminated from Eq. (12) using Eqs. (5) and (6). After eliminating the normal contact force $\mathbf{N}$, Eq. (12) can be solved efficiently with an iterative solution method.

Once the equilibrium position for steady sliding is found, friction forces and contact forces on the sliding surfaces can be recovered according to Eqs. (1) and (2). The equations for dynamic motion near the equilibrium position can be established by replacing $\mathbf{X}$, $\mathbf{F}$ and $\mathbf{N}$ with $\mathbf{X}+\mathbf{x}$, $\mathbf{F}+\Delta\mathbf{F}$ and $\mathbf{N}+\Delta\mathbf{N}$ and adding inertia and damping terms in Eqs. (1)–(6). After simplification, the following equations can be derived:

$$\sum_{j=1}^{n} M_{ij}\ddot{x}_j+\sum_{j=1}^{n} C_{ij}\dot{x}_j+\sum_{j=1}^{n} K_{ij}x_j=\Delta F_i,\quad i=1,2,\ldots,2m \tag{13}$$

$$\sum_{j=1}^{n} M_{ij}\ddot{x}_j+\sum_{j=1}^{n} C_{ij}\dot{x}_j+\sum_{j=1}^{n} K_{ij}x_j=\Delta N_i,\quad i=2m+1,2m+2,\ldots,4m \tag{14}$$

$$\sum_{j=1}^{n} M_{ij}\ddot{x}_j+\sum_{j=1}^{n} C_{ij}\dot{x}_j+\sum_{j=1}^{n} K_{ij}x_j=0,\quad i=4m+1,4m+2,\ldots,n \tag{15}$$

$$\Delta F_i+\Delta F_{i+m}=0,\quad i=1,2,\ldots,m \tag{16}$$

$$\Delta N_i+\Delta N_{i+m}=0,\quad i=2m+1,2m+2,\ldots,3m \tag{17}$$

$$X_i-X_{i+m}=0,\quad i=2m+1,2m+2,\ldots,3m \tag{18}$$

where $\mathbf{M}$ is the mass matrix, $\mathbf{C}$ the damping matrix, and $\Delta\mathbf{F}$ and $\Delta\mathbf{N}$ are the dynamic increments of friction force and normal contact force vectors, respectively. The relationship between $\Delta\mathbf{F}$ and $\Delta\mathbf{N}$ can be derived from the friction law. For the master nodes with the normal axis pointing to the inside of the master component, the following equations can be established:

$$F_i+\Delta F_i=\mu_{i\Delta}(N_{i+2m}+\Delta N_{i+2m}),\quad i=1,2,\ldots,m \tag{19}$$

$$\mu_{i\Delta}=\mu_s+\alpha(V_i-\dot{x}_i+\dot{x}_{i+m})=\mu_i-\alpha(\dot{x}_i-\dot{x}_{i+m}),\quad i=1,2,\ldots,m \tag{20}$$

Inserting Eq. (20) in Eq. (19) and utilizing Eq. (7), one obtains

$$\Delta F_i=\mu_i\Delta N_{i+2m}-\alpha N_{i+m}(\dot{x}_i-\dot{x}_{i+m}),\quad i=1,2,\ldots,m \tag{21}$$

Combining Eqs. (14) and (21) results in an expression for ΔF_i containing the first and second terms of x. For eigenvalue analysis, the following equations for master nodes can be derived when ΔF_i is inserted in Eq. (13) after the second term is ignored:

$$\sum_{j=1}^{n}(M_{ij}-\mu_i M_{i+2m,j})\ddot{x}_j+\sum_{j=1}^{n}(C_{ij}-\mu_i C_{i+2m,j})\dot{x}_j+\alpha N_{i+2m}(\dot{x}_i-\dot{x}_{i+m})+\sum_{j=1}^{n}(K_{ij}-\mu_i K_{i+2m,j})x_j=0,\quad i=1,2,\ldots,m \tag{22}$$

Following the same approach, the equations for the slave nodes can be obtained:

$$\sum_{j=1}^{n}(M_{ij}-\mu_i M_{i+2m,j})\ddot{x}_j+\sum_{j=1}^{n}(C_{ij}-\mu_i C_{i+2m,j})\dot{x}_j-\alpha N_{i+2m}(\dot{x}_i-\dot{x}_{i-m})+\sum_{j=1}^{n}(K_{ij}-\mu_i K_{i+2m,j})x_j=0,\quad i=m+1,m+2,\ldots,2m \tag{23}$$

Eqs. (22), (23) and (14), (15) can be compacted to a matrix form as below:

$$(\mathbf{M}-\mathbf{M}_f)\ddot{x}+(\mathbf{C}+\mathbf{C}_f+\mathbf{C}_\alpha)\dot{x}+(\mathbf{K}+\mathbf{K}_f)x=\Delta\mathbf{N} \tag{24}$$

Matrices $\mathbf{M}_f$, $\mathbf{C}_f$, $\mathbf{C}_\alpha$ and $\mathbf{K}_f$, which represent effects of friction on dynamics of the system near the equilibrium position, are determined according to Eqs. (22) and (23). The dynamic increment $\Delta\mathbf{N}$ in normal forces and the first m DOFs x_i, $i=1, 2, \ldots, m$ can be eliminated from Eq. (24) using Eqs. (17) and (18). After the elimination process, the equations of motion can be reduced to the following form:

$$\mathbf{M}_r\ddot{x}+\mathbf{C}_r\dot{x}+\mathbf{K}_r x=0 \tag{25}$$

where $\mathbf{M}_r$, $\mathbf{C}_r$ and $\mathbf{K}_r$ are $(n-m)$ by $(n-m)$ asymmetric matrices. The eigenavlue equation of Eq. (25) is given as follows:

$$(\mathbf{M}_r\lambda^2+\lambda\mathbf{C}_r+\mathbf{K}_r)\varphi=0 \tag{26}$$

The general solution of Eq. (25) is

$$x(t) = \sum \boldsymbol{\varphi}_i \exp(\lambda_i t) = \sum \boldsymbol{\varphi}_i \, exp((\alpha_i + \mathrm{j}\omega_i)t) \tag{27}$$

where $\boldsymbol{\varphi}_i$ is the ith eigenvector of Eq. (26) and $\lambda_i = \alpha_i + \mathrm{j}\omega_i$ the ith eigenvalue of Eq. (26); j is the imaginary unit. From Eq. (27), it is seen that when the real part of an eigenvalue is larger than zero, displacement will increase with time, that is, vibration of the system becomes unstable.

Eqs. (1)–(27) constitute the analysis theory of self-excited vibration of frictional systems. Similar to friction brake systems, the finite element stability analysis of a wheelset–track system in the presence of friction (saturated creep force) is very complicated and difficult [33–36]. Many efforts have been made to make it easier. Recently, ABAQUS versions 6.4 and above provide a complex eigenvalue solution to the stability analysis of friction-induced vibration problems. This new capability uses direct contact coupling at the contact interface described by Ouang et al. [33]. In the present paper, ABAQUS's complex eigenvalue analysis capability is applied to study stability of the wheelset–track system. The main procedure for applying ABAQUS to perform the complex eigenvalue analysis of the wheelset–track system is given as follows:

(1) nonlinear static analysis of the wheelset–track system for applying suspension forces,
(2) nonlinear static analysis to impose sliding speed on the wheelset,
(3) normal mode analysis to extract natural frequencies without friction coupling,
(4) complex eigenvalue analysis that incorporates the effect of friction coupling.

2.3. Finite element model of a wheelset–track system

From Fig. 2, it is seen that there are two distinct contact conditions for the high and low rails. Therefore these two contact conditions must be established in modeling the wheelset–track system. Fig. 4 shows a solid model and two finite element models of the wheelset–track system. In the finite element models, a rail length of 36 m is chosen for end effects to be negligible. In the models, hinged–hinged constraints of rail ends are used. The distance between two adjacent sleepers is 600 mm. The width of sleepers is 160 mm. The rails are supported by a group of lateral and vertical springs and

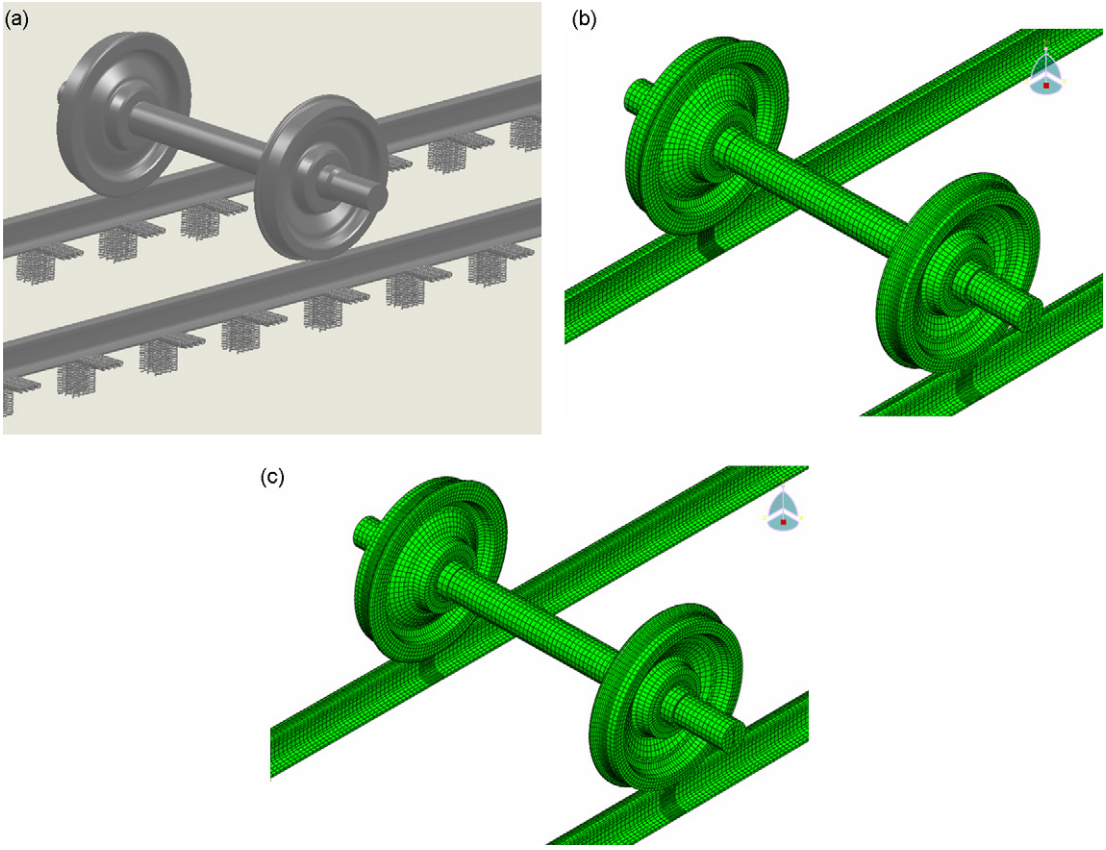

Fig. 4. Model of the wheelset–track system: (a) solid model of the wheelset–track system, (b) finite element model of the wheelset–track system on a tight curved track and (c) finite element model of the wheelset–track system on a straight track.

a group of lateral and vertical dampers at each position of sleepers. The number of lateral or vertical springs in each group of springs is the same as the number of rail nodes on the contact interface between the rail and each sleeper. A wheel with worn tread profile of a freight car of nominal diameter 840 mm is analyzed. The rail mass is 60 kg/m.

2.4. Corrugation wear analysis

In this section, self-excited vibration of the wheelset–track system will be related to corrugation generation. In the literature, it is generally accepted that fluctuating friction work results in undulant wear of rails [7,8]. Brockley [21] proposed a modified wear equation as follows:

$$w = K(H-C) \tag{28}$$

where w is the wear volume per unit time, K the wear constant, H the friction work rate (equals FV), F the creep force, V the relative velocity and C the durability friction work rate.

Eq. (28) may be applied to explain corrugation formation due to self-excited vibration of the wheelset–track system. When the lateral creep force F is saturated, $F=\mu N$, where μ is the friction coefficient between the wheel and rail and N the normal contact force. Lateral velocity of the wheelset V is equal to ψ multiplied by v, where ψ the angle of attack of the wheelset and v the forward speed of the wheelset. When a vehicle negotiates a sharply curved track in a steady state, μ, ψ and v may be considered to be constant. In the present work, transient response of self-excited vibration of the wheelset–track system is not analyzed. The reason is partially that transient response analysis of such a self-excited vibrating system is a formidable task. Based on the understanding of friction-induced vibration, self-excited vibration is predicted by the complex eigenvalue approach and the self-excitation mechanism is known as mode coupling [33–36], which is well known and has been accepted in the dynamics community for other friction-induced vibration problems, such as brake squeal. In mode coupling vibration, the tangential vibration component of the system is coupled with the normal vibration component. This suggests that when such self-excited vibration occurs, normal force fluctuates. Several transient analysis results support the conclusion [37]. In this paper, it is accepted that normal contact force fluctuates when self-excited vibration occurs. Therefore it is deduced that friction work rate H fluctuates when self-excited vibration occurs. According to Brockley [21], such a fluctuating friction work rate can result in rail corrugation.

2.5. Nominal parameters of the wheelset–track system

Density of the wheel and rail materials is $\rho=7800$ kg/m^3. Young's modulus of both is $E=2.1\times10^{11}$ N/m. Poisson's ratio of both is $\gamma=0.3$. In the present work, speed of the vehicle running on a curved track is set to $v=70$ km/h. A curved track of radius 300 m with a superelevation of 110 mm and a rail cant 1/40 is chosen. The wheelbase gauge of a wheelset is 1750 mm. Vertical, lateral and longitudinal spring stiffness values of the bogie primary suspension are 1.75×10^8, 3.5×10^8 and 3.68×10^8 N/m, respectively. Vertical, lateral and longitudinal damping values of the bogie primary suspension are 1.63×10^3, 1.24×10^3 and 1.24×10^3 Ns/m, respectively. Based on the NUCARS simulation, it is found that when the vehicle negotiates the curved track at a speed of 70 km/h, the contact angles are $\delta_L=36.41^\circ$ and $\delta_R=1.52^\circ$. Angle of attack of the leading wheelset is $y_w=0.30^\circ$. The suspension forces are $F_{SVL}=103{,}200$ N, $F_{SVR}=91{,}800$ N, $F_{SLL}=7640$ N and $F_{SLR}=7640$ N. On a straight track, it is assumed that the contact angles are $\delta_L=4.26^\circ$ and $\delta_R=4.26^\circ$, and suspension forces $F_{SVL}=100{,}000$ N, $F_{SVR}=100{,}000$ N, $F_{SLL}=0$ and $F_{SLR}=0$. Stiffnesses of a sleeper support are set to $k_L=11.18\times10^6$ N/m and $k_V=34.5\times10^6$ N/m [18,38]. In the present work, damping matrix $\mathbf{C}$ in Eq. (24) is neglected. Without damping, instability caused by mode coupling can be revealed more clearly.

3. Results and discussion

3.1. Mode shapes of self-excited vibration of the wheelset–track system

Generally, the frequency of rail corrugation is considered to fall in the range 20–1200 Hz. Therefore the present results are limited to this frequency range. The effective damping ratio is defined as $\zeta=-2R_e(\lambda)/|I_m(\lambda)|$, which is a parameter to measure propensity of self-excited vibration occurrence. The smaller the effective damping ratio, the easier the corresponding self-vibration. For the wheelset–track system shown in Fig. 4, the complex eigenvalue analysis shows that there are five unstable modes when friction coefficient $\mu=0.4$ with no damping in the sleeper support. In the present work, only those modes whose damping ratios are less than -0.001 are given. It needs to be noted that if a damping ratio is not less than -0.001, its corresponding unstable vibration is considered unlikely to occur. That is because there is always enough structural damping to overcome this small amount of negative damping, which is not taken into account in the present complex eigenvalue analysis in order to better understand the mode coupling mechanism of the wheelset–track system. In Section 3.2, the effect of damping of sleeper supports on self-excited vibration of the wheelset–track system will be discussed. Fig. 5 shows these five unstable mode shapes. From Fig. 5a, b and e it is seen that self-excited vibration most probably takes place on the high rail and the wheel. From Fig. 5c it is seen that self-excited vibration also probably takes place on both rails and the two wheels. From Fig. 5d it is seen that self-excited vibration also probably takes place only on

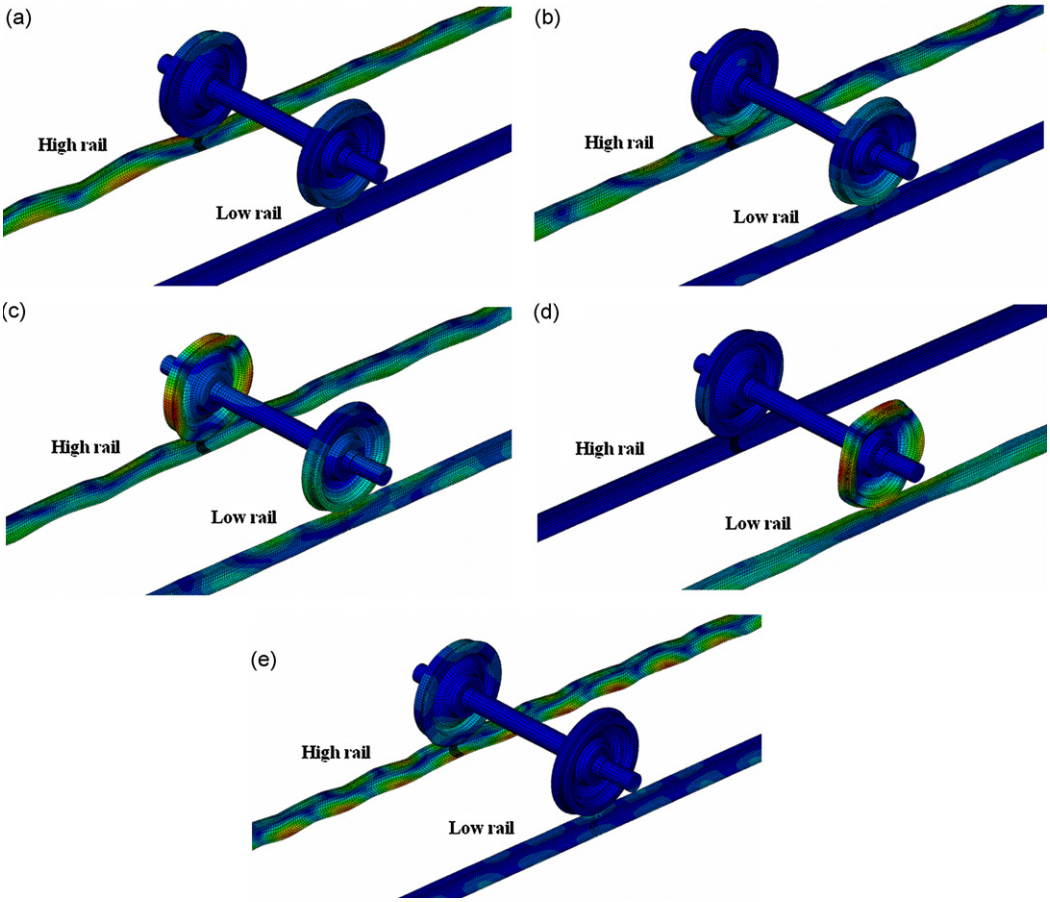

Fig. 5. Mode shapes of unstable vibrations on a tight curve track, friction coefficient μ=0.4, C_V=0, C_L=0, k_L=11.18 × 10^6 N/m and k_V=34.5 × 10^6 N/m: (a) unstable vibration frequency f_R=315.36 Hz, damping ratio ζ= −0.005, (b) f_R=381.28 Hz, ζ= −0.004, (c) f_R=431.84 Hz, ζ= −0.009, (d) f_R=477.57 Hz, ζ= −0.040 and (e) f_R=798.79 Hz, ζ= −0.004.

the low rail and the wheel. It is found that the mode shown in Fig. 5d has a damping ratio of $\zeta = -0.040$. This damping ratio is the least among all these five damping ratios of unstable modes and suggests that the mode shown in Fig. 5d most easily occurs. The frequency of unstable vibration is f_R=477.57 Hz. The wavelength of the corresponding rail corrugation is l=0.0407 m (forward speed of the vehicle v=70 km/h), which is a short wavelength corrugation. Therefore from Fig. 5 it may be inferred that a short wavelength rail corrugation on tight curves most probably takes place on the low rail. The conclusion is consistent with field results of railway lines [16]. It needs to be mentioned that no mode shapes shown in Fig. 5 seem to include wheelset torsion, based on the animation of these mode shapes.

Trains undergo very large longitudinal traction forces or brake forces when they are accelerated or are braked. If these longitudinal traction forces or brake forces become saturated, that is, equal to the normal forces multiplied by the dynamic coefficient of friction, these saturated creep forces also can induce self-excited vibration of the wheelset–track system. Fig. 6 shows the mode shapes of unstable vibration on a straight track. The wavelength of corrugation on tangent tracks is evaluated to be l=0.077 m for the unstable frequency f_R=431.50 Hz at a speed of 120 km/h and l=0.054 m for the unstable frequency f_R=614.62 Hz at a speed of 120 km/h. It needs to be mentioned that no mode shapes shown in Fig. 6 seem to include wheelset torsion, based on animation of these mode shapes.

In the railway research community, stability of the wheelset–track system due to friction (saturated creep force) coupling sounds very strange. However, it is well known in the tribology research community that friction can induce vibration and noise. Up to now, the generation mechanism of friction-induced vibration is still not fully understood in the tribology community [33–36]. This suggests that the mechanism behind friction-induced vibration is very elusive. Nowadays, finite element complex eigenvalue analysis is thought to be an effective and matured method available to predict squeal propensity of friction sliding systems [33]. In the present paper, finite element complex eigenvalue analysis is applied to study stability of the wheelset–track system due to the saturated creep force coupling. To the authors' knowledge, this is the first work to propose that saturated creep force can induce self-excited vibration in a wheelset–track system in some conditions. This work brings a new insight to the rail corrugation generation mechanism.

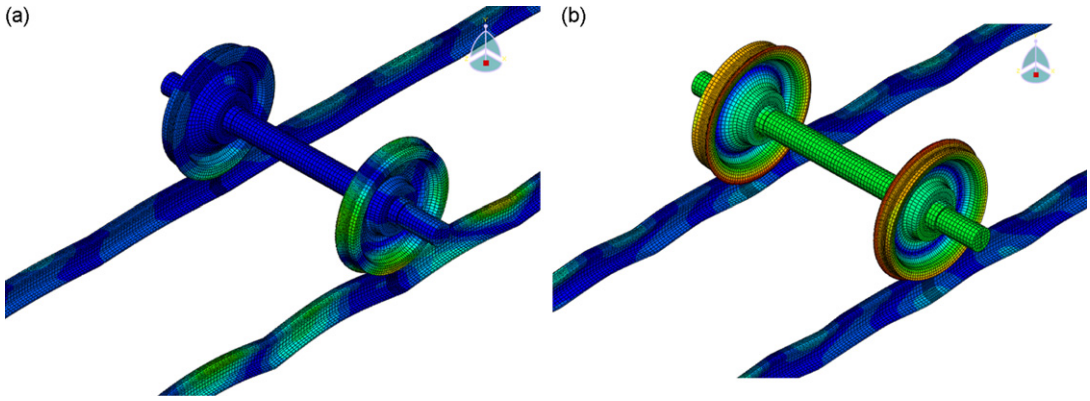

Fig. 6. Mode shapes of unstable vibrations on a straight track, μ=0.4, C_V=0, C_L=0, k_L=11.18 × 10^6 N/m, k_V=34.5 × 10^6 N/m: (a) f_R=431.50 Hz, ζ = −0.0007 and (b) f_R=614.62 Hz, ζ = −0.0022.

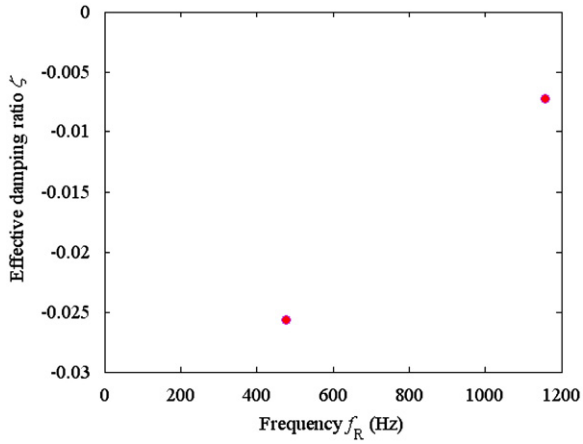

Fig. 7. Unstable frequencies of vehicle travelling on curved track with sleeper, μ=0.4, C_L=27,300 Ns/m, C_V=14,500 Ns/m, k_L=11.18 × 10^6 N/m and k_V=34.5 × 10^6 N/m.

3.2. *Effect of sleeper support damping on self-excited vibration of the wheelset–track system*

Sleeper support damping has a significant effect on self-excited vibration of the wheelset–track system. In the present work, a series of lateral and vertical linear damping elements are added between the ground and each node on rail surfaces, where they come into contact with the sleepers. The total linear damping force on each rail surface is assumed to be F_{DL}=$C_L V_L$ for the lateral sleeper support damping elements and F_{DV}=$C_V V_V$ for the vertical sleeper support damping elements, where F_{DL} and F_{DV} are the lateral and vertical sleeper support damping forces, respectively. V_L and V_V are the lateral and vertical velocities of each node on the rail surfaces with respect to the ground, respectively. Fig. 7 shows the distribution of unstable frequencies in the presence of sleeper support damping. From Fig. 7, it is seen that there are only two negative damping ratios in the presence of sleeper support damping. The mode shapes associated with these two negative damping ratios are shown in Fig. 8. Comparing Fig. 5d with Fig. 8a, it is seen that the main mode shape of self-excited vibration with sleeper support damping is very similar to that without sleeper support damping. Under these two conditions, all unstable vibrations take place on the low rail and the wheel. Comparing Fig. 5 with Fig. 8, it is seen that the number and absolute values of negative effective damping ratios with sleeper support damping are much less than those without sleeper support damping. This result suggests that sleeper support damping can greatly reduce propensity of self-excited vibrations of the wheelset–track system. Therefore sleeper support damping can greatly suppress rail corrugation. A further analysis demonstrates that sleeper support damping cannot eliminate all self-excited vibrations of the wheelset–track system even when damping is made four times the nominal value. Fig. 9 shows a group of results. From Fig. 9, it is seen that when C_L=0, 5454.5, 54,545, 109,090 Ns/m and C_V=14,500 Ns/m, or when C_L=27,300 Ns/m, C_V=0, 2900, 29,000 and 58,000 Ns/m, there is always self-excited vibration of frequency at about 476.7 Hz. Comparing Fig. 5 with Fig. 9, it is found that lateral and vertical dampings of the sleeper supports have an obvious influence on self-excited vibrations of the wheelset–track system. It is seen that if lateral and vertical dampings of the sleeper supports are too small, more self-excited vibrations will probably take place.

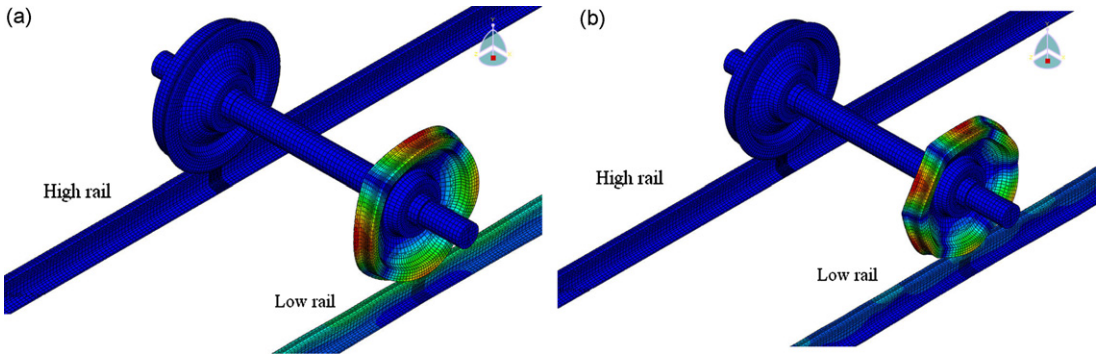

Fig. 8. Mode shapes of unstable vibrations shown in Fig. 7: (a) f_R=476.70 Hz, $\zeta=-0.026$ and (b) f_R=1157.4 Hz, $\zeta=-0.007$.

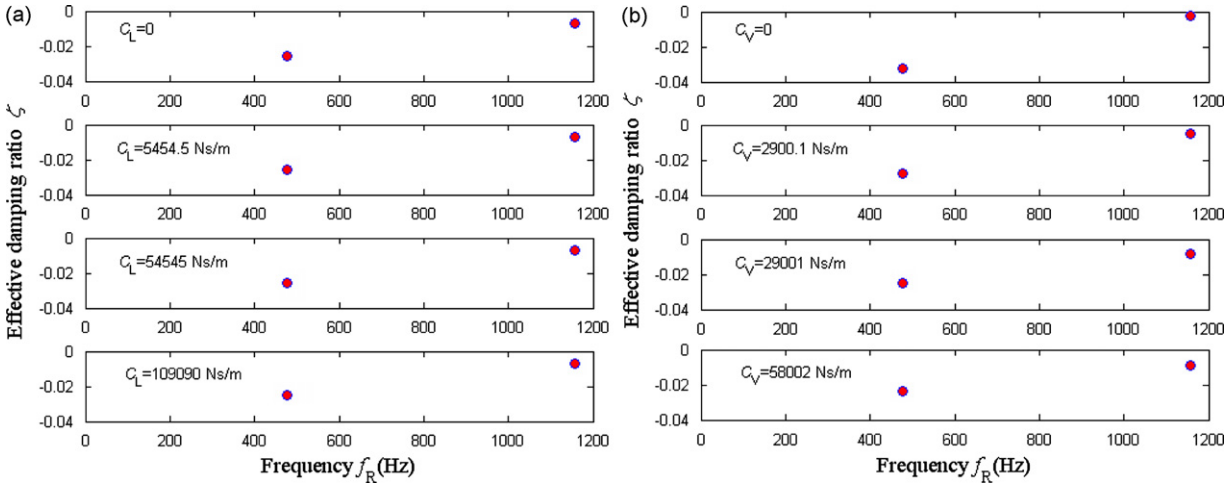

Fig. 9. Distribution of unstable frequencies with sleeper support damping on curved track, μ=0.4, $k_L=11.18\times10^6$ N/m, $k_V=34.5\times10^6$ N/m: (a) C_V=14,500 Ns/m and (b) C_L=27,300 Ns/m.

3.3. *Effect of friction coefficient on self-excited vibration of the wheelset–track system*

Friction coupling is generally considered to be a main cause of self-excited vibration of frictional systems. Obviously the larger the coefficient of friction, the stronger the friction coupling. Therefore the coefficient of friction has a big influence on self-excited vibration of wheelset–track systems. Fig. 10 shows variation of the damping ratio ζ with friction coefficient μ between the wheel and the rail. It needs to be mentioned that when $\mu<0.21$ no unstable self-excited vibration of the wheelset–track system is predicted. From Fig. 10a, it is found that when the friction coefficient μ=0.21 there is a small effective damping ratio whose value is -0.00064. From Fig. 10b, it is seen that when μ=0.8 there are 5 negative damping ratios whose values are less than 0 and larger than -0.082. Comparing Fig.10 with Fig. 7, it is also found that with increasing friction coefficient, the number of negative damping ratios increases and the maximum absolute values of negative damping ratios increase. This suggests that with increasing friction coefficient, rail corrugation occurs more easily. This conclusion is consistent with the test results [27–29].

3.4. *Effect of stiffness of the sleeper support spring on self-excited vibration of the wheelset–track system*

Fig. 11 shows distributions of unstable frequencies at several stiffness values of sleeper support springs. Comparing Fig. 7 with Fig. 11, it is found that stiffness of the sleeper support springs has an influence on self-excited vibration of a wheelset–track system. From Fig. 11a and b, it is seen that when stiffness of the sleeper support springs is set to $k_V=14.4\times10^6$ N/m, $k_L=11.18\times10^6$ N/m or $k_V=40\times10^6$ N/m, $k_L=11.18\times10^6$ N/m, the wheelset–track system has two self-excited unstable frequencies. From Fig. 11c, it is seen that when stiffness of the sleeper support springs is set to $k_V=58.8\times10^6$ N/m, $k_L=29.4\times10^6$ N/m, the unstable frequencies of the wheelset–track system become 506.66 and 704.09 Hz.

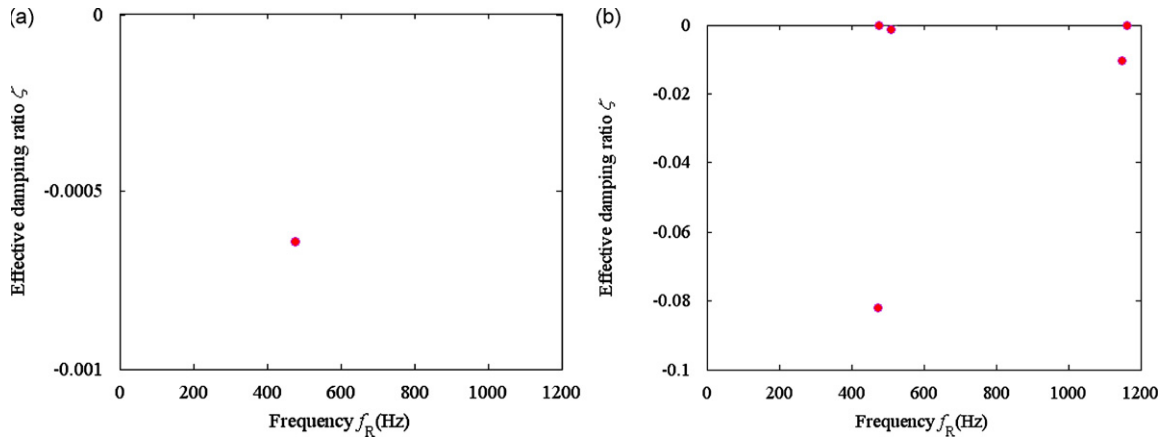

Fig. 10. Distributions of unstable frequencies on curved track, $k_L=11.18\times10^6$ N/m, $k_V=34.5\times10^6$ N/m, $C_V=14{,}500$ Ns/m and $C_L=27{,}300$ Ns/m: (a) $\mu=0.21$, $\delta_L=15.28^\circ$, $\delta_R=1.69^\circ$ and (b) $\mu=0.8$.

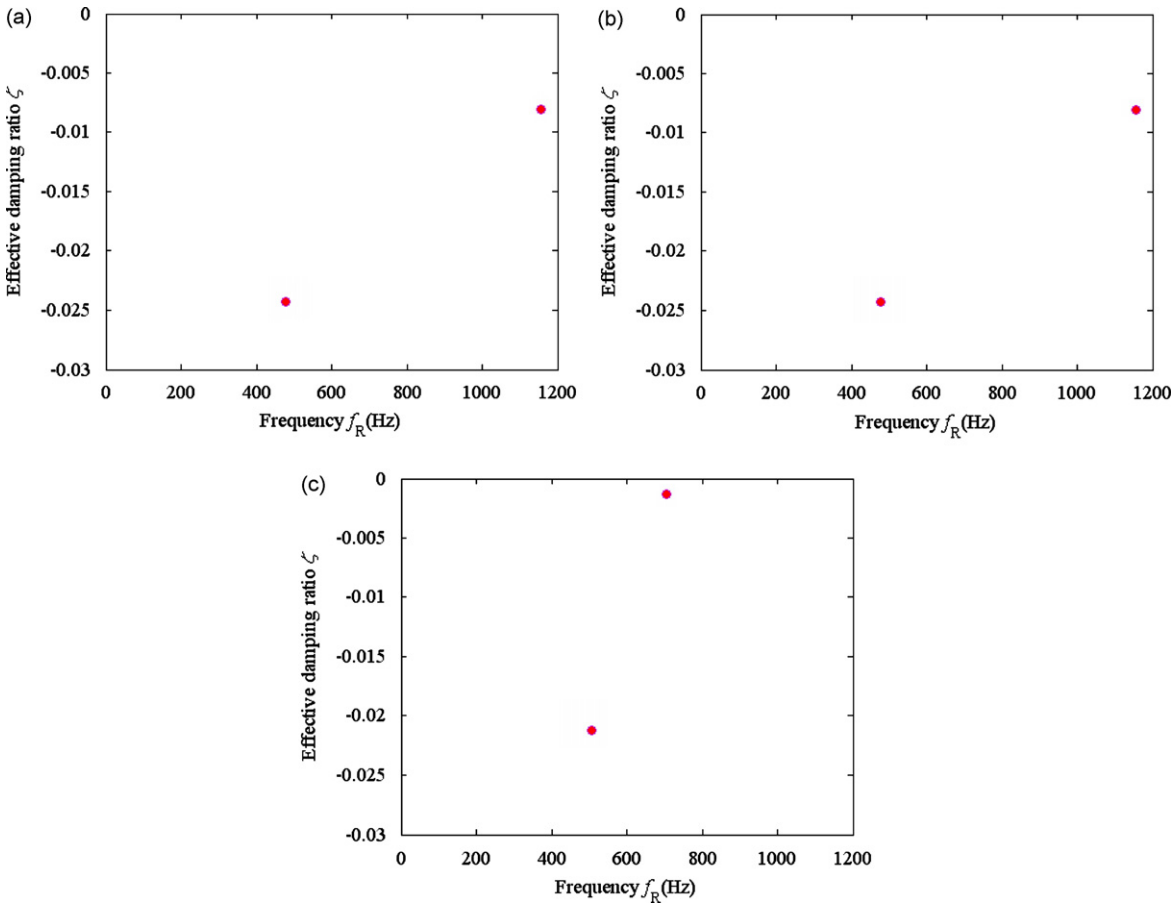

Fig. 11. Distributions of unstable frequencies on curved track, $\mu=0.4$, $C_V=14{,}500$ Ns/m and $C_L=27{,}300$ Ns/m: (a) $k_V=14.4\times10^6$ N/m, $k_L=11.18\times10^6$ N/m, (b) $k_V=48\times10^6$ N/m, $k_L=11.18\times10^6$ N/m and (c) $k_V=58.8\times10^6$ N/m, $k_L=29.4\times10^6$ N/m.

3.5. *Effect of friction–velocity slope on self-excited vibration of the wheelset–track system*

Eadie et al. [27] reported that the FM technique can suppress rail corrugation. Eadie's conclusion may be reexamined by applying the present complex eigenvalue approach. In ABAQUS package, two data points are given to fit the exponential

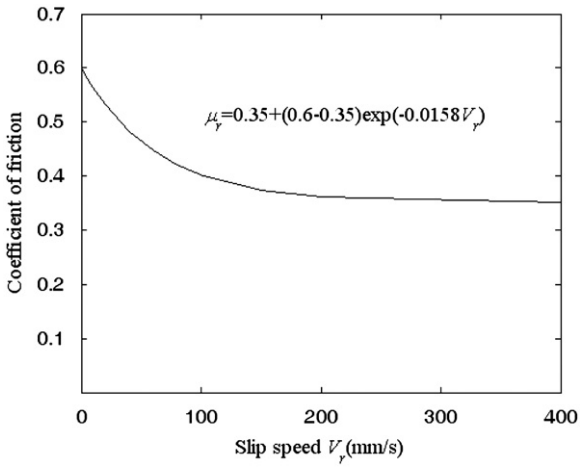

Fig. 12. Friction–velocity relationship.

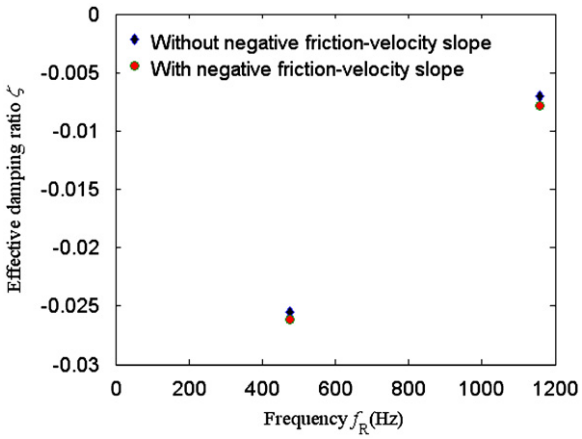

Fig. 13. Effect of negative friction–velocity slope on self-vibration of wheelset–track system on the curved track, μ=0.4, C_V=14,500 Ns/m, C_L=27,300 Ns/m, k_L=11.18 × 10^6 N/m and k_V=34.5 × 10^6 N/m.

model of friction. The first point μ_s represents static coefficient of friction specified at relative speed V_r=0, and the second point, (V_r, μ_r), corresponds to an experimental measurement taken at a relative speed V_r. The fitted friction–velocity model is shown in Fig. 12. When the lateral sliding speed of the wheelset as a result of angle of attack is $V_r=\psi V=0.30\times 3.14/180\times 70/3.6$ m/s=0.102 m/s and the dynamic coefficient of friction predicted by the friction model shown in Fig. 12 is μ_r=0.4. Fig. 13 shows a comparison between results with and without negative friction–velocity slope. From Fig. 13 it is seen that values of negative damping ratios with negative friction–velocity slope are less than those without negative friction–velocity slope. This result suggests that negative friction–velocity slope more easily leads to self-excited vibration of the wheelset–track system, and therefore rail corrugation. This conclusion is consistent with Eadie's test results [27]. However, from Fig. 13, it is found that there is a small difference in negative damping ratio under these two conditions. This suggests that negative friction–velocity slope has a small effect on unstable vibration of wheelset–track systems.

4. Conclusions

The present work studies the formation mechanism of rail corrugation from the viewpoint of saturated-creep-force-induced self-excited vibration of a wheelset–track system. A finite element model consisting of a wheelset, track and rail support springs and dampers is established and analyzed. In the model, it is assumed that creep forces between wheels and rails are saturated, which is a realistic assumption when the wheelset negotiates a sharp curve as well as on straight track during traction and braking. Several sensitivity analyses of self-excited vibration of a wheelset–track system are carried out. The following conclusions can be drawn.

The saturated creep force can cause self-excited vibration of the wheelset–track system when the friction coefficient between the wheels and rails is above 0.21. This self-excited vibration is probably responsible for rail corrugation. Coefficient of friction between the wheel and the rail has an important effect on self-excited vibration of the wheelset–track system and therefore on the occurrence of rail corrugation. Propensity of rail corrugation occurrence increases with increasing coefficient of friction. Sleeper support damping has a big effect on occurrence of rail corrugation and may suppress rail corrugation. Negative friction–velocity slope has a small influence on occurrence of rail corrugation.

Acknowledgement

The authors gratefully thank Mr. Wang G.X. for his help in revision of the manuscript. The authors thank financial supports from National Natural Science Foundation of China (no. 50875220), Innovative Research Group Program of National Natural Science Foundation of China (no. 50821063), State Key Development Program of Basic Research of China (no. 2007CB714700), Innovative Research Group Program of Southwest Jiaotong University (no. 2007IRT01) and Self-determined and Innovative Research Program of the State Key Laboratory of Traction and Power, Southwest Jiaotong University (no. 2009TPL-03).

References

[1] S.L. Grassie, J. Kalousek, Rail corrugation: characteristics, causes and treatments, *Journal of Rail Rapid Transit* 207 (1993) 57–68.
[2] S.L. Grassie, Rail corrugation: advances in measurement, understanding, and treatment, *Wear* 258 (2005) 1224–1234.
[3] Y. Sato, A. Matsumoto, K. Knothe, Review on rail corrugation studies, *Wear* 253 (2002) 130–139.
[4] D.K. Ahlbeck, L.E. Daniels, A review of rail corrugation processes under different operating modes, in: Proceedings of the ASME Joint Railroad Conference, 1990, pp. 13–18.
[5] K. Knothe, *Non-steady state rolling contact and corrugations*, *Rolling Contact Phenomena (CISME Courses and Lectures)*, Springer, New York, 2000 pp. 203–276.
[6] K.H. Oostermeijer, Review on short pitch rail corrugation studies, *Wear* 265 (2008) 1231–1237.
[7] K. Hempelmann, K. Knothe, An extended linear model for the prediction of short pitch corrugation, *Wear* 191 (1996) 161–169.
[8] A. Igeland, H. Ilias, Railhead corrugation growth predictions based on nonlinear high frequency vehicle/track interaction, *Wear* 213 (1997) 90–97.
[9] A. Matsumoto, Y. Sato, et al., Study on the formation mechanism of rail corrugation on curved track, *Vehicle System Dynamics* 25 (1996) 450–465.
[10] E.G. Vadillo, J.A. Tarrago, G.G. Zubiaurre, C.A. Duque, Effect of sleeper distance on rail corrugation, *Wear* 217 (1998) 140–146.
[11] H. Ilias, The influence of railpad stiffness on wheelset/track interaction and corrugation growth, *Journal of Sound and Vibration* 227 (5) (1999) 935–948.
[12] S. Muller, A linear wheel–rail model to investigate stability and corrugation on straight track, *Wear* 249 (2001) 1117–1127.
[13] J.B. Nielsen, Evolution of rail corrugation predicted with a non-linear model, *Journal of Sound and Vibration* 227 (5) (1999) 915–933.
[14] C. Andersson, A. Johansson, Prediction of rail corrugation generated by three-dimensional wheel–rail interaction, *Wear* 257 (2004) 423–434.
[15] T.X. Wu, D.J. Thompson, Vibration analysis of railway track with multiple wheels on the rail, *Journal of Sound and Vibration* 239 (2001) 69–97.
[16] X.S. Jin, Z.F. Wen, K.Y. Wang, Effect of track irregularities on initiation and evolution of rail corrugation, *Journal of Sound and Vibration* 285 (1–2) (2005) 121–148.
[17] X.S. Jin, Z.F. Wen, K.Y. Wang, Z.R. Zhou, Q.Y. Liu, C.H. Li, Three-dimensional train–track model for study of rail corrugation, *Journal of Sound and Vibration* 293 (3–5) (2006) 830–855.
[18] X.S. Jin, Z.F. Wen, Effect of discrete track support by sleepers on rail corrugation at a curved track, *Journal of Sound and Vibration* 315 (2008) 279–300.
[19] R.A. Clark, Slip–stick vibrations may hold the key to corrugation puzzle, *Railway Gazette International* 7 (1984) 531–533.
[20] R.A. Clark, G.A. Scott, W. Poole, Short wave corrugation—an explanation based on stick–slip vibrations, in: Proceedings of the Applied Mechanics Rail Transportation Symposium 96, ASME, 1988, pp. 141–148.
[21] C.A. Brockley, An investigation of rail corrugation using friction-induced vibration theory, *Wear* 128 (1988) 99–106.
[22] M. Ishida, T. Moto, M. Takikawa, The effect of lateral creepage force on rail corrugation on low rail at sharp curves, *Wear* 253 (2002) 172–177.
[23] Mitsuo Yoshihiro Suda, Mikio Hanawa, Takashi Okumura, Iwasa, Study on rail corrugation in sharp curves of commuter line, *Wear* 253 (2002) 193–198.
[24] Akira Matsumoto, Yasuhiro Sato, Hiroyuki Ono, Masuhisa Tanimoto, et al., Formation mechanism and countermeasures of rail corrugation on curved track, *Wear* 253 (2002) 178–184.
[25] T.X. Wu, D.J. Thompson, An investigation into rail corrugation due to micro-slip under multiple wheel/rail interactions, *Wear* 258 (2005) 1115–1125.
[26] Y.Q. Sun, S. Simson, Wagon–track modeling and parametric study on rail corrugation initiation due to wheel stick–slip process on curved track, *Wear* 265 (2008) 1193–1201.
[27] D.T. Eadie, M. Santoro, K. Oldknow, Y. Oka, Field studies of the effect of friction modifiers on short pitch corrugation generation in curves, *Wear* 265 (2008) 1212–1221.
[28] M. Tomeoka, N. Kabe, M. Tanimoto, E. Miyauchi, M. Nakata, Friction control between wheel and rail by means of on-board lubrication, *Wear* 253 (2002) 124–129.
[29] D.T. Eadie, J. Kalousek, K.C. Chiddick, The role of high positive friction (HPF) modifier in the control of short pitch corrugations and related phenomena, *Wear* 253 (2002) 185–192.
[30] W.J.T. Daniel, C.Y. Cheng, P.A. Meehan, Modelling the effects of friction modifiers on rail corrugation in cornering, *Vehicle System Dynamics* 46 (2008) 845–866.
[31] V.K. Garg, R.V. Dukkipati, *Dynamics of Railway Vehicle Systems*, Academic press, New York, USA, 1984.
[32] F.B. Blader, J.A. Elkins, N.G. Wilson, P.E. Klauser, Development and validation of a general railroad vehicle dynamics simulation (NUCARS), in: Proceedings of the ASME/IEEE Joint Railroad Conference, Philadelphia, PA, April, 1989.
[33] H. Ouyang, W. Nack, Y. Yuan, F. Chen, Numerical analysis of automotive disc brake squeal: a review, *International Journal of Vehicle Noise Vibration* 1 (3/4) (2005) 207–231.
[34] G.D. Liles, Analysis of disc brake squeal using finite element methods, 1989, SAE Paper 891150.
[35] W.V. Nack, Brake squeal analysis by finite elements, *International Journal of Vehicle Design* 23 (2000) 263–275.
[36] Y. Yuan, An eigenvalue analysis approach to brake squeal problem, in: Proceedings of the 29th ISATA Conference Automotive Braking Systems, 1996, Florence, Italy.
[37] F. Massi, L. Baillet, O. Giannini, A. Sestieri, Brake squeal: linear and nonlinear numerical approaches, *Mechanical Systems and Signal Processing* 21 (2007) 2374–2393.
[38] Lei Xiaoyan, *New Methods in Railroad Track Mechanics and Technology*, China Railway Publishing House, Beijing, 2002 (in Chinese).